Palmprint Identification using PalmCodes

Ajay Kumar[1,2], Helen C. Shen[1]
[1]*Department of Computer Science, Hong Kong University of Science & Technology*, *Hong Kong*
[2]*Department of Computing, The Hong Kong Polytechnic University*, *Hong Kong*
E-mail: *ajaykr@ieee.org*, *helens@cs.ust.hk*

Abstract

This paper investigates a new approach for the palmprint identification using Real Gabor Function (RGF) filtering. Inkless composite hand images have been used to automatically extract the palmprints from peg-free imaging setup. These palmprints, after normalization, are subjected to selective feature sampling by a bank of RGF. Each of these filtered images has been used to extract significant features (*PalmCode*) *from each of 6 concentric circular bands. Our preliminary experimental results using 400 low-resolution palmprint images achieve the recognition rate of 97.50% and also illustrate the shortcomings of results presented in earlier work. The results show the uniqueness of palmprint texture, even in the two hands of an individual and its possible use in biometrics based personal recognition.*

1. Introduction

The first commercial palmprint identification system [1] was developed in 1971 which was followed by another system from IBM in 1977 [2]. Most of the prior work [1]-[3] on palmprint identification has been focused on the principal palmprint features *i.e.* creases and lines. However, a palmprint image can also be analyzed as texture, which is random rather than uniform. The multichannel filtering of every palmprint image using only real Gabor functions, instead of complex Gabor functions used in [4], can be employed to capture its salient features. Any commercial development of an automated palmprint based identification system would require automated extraction of region of interest *i.e.* palmprint area, while ignoring fingers, wrist, and background (if any). This paper also presents an elegant and simple method for the automated selection of palmprint area from the composite hand image.

2. System Overview

The block diagram for the complete recognition system is shown in figure 1. The composite hand image from the users is used to select the palmprint. These palmprints are subjected to normalization. The normalization is used to reduce the brightness and contrast variations due to sensor noise and variations in palm pressure. Each of the normalized images is further subjected to multichannel filtering using a bank of RGF filters. Each of the filtered images is used to compute the salient features in several concentric overlapping bands. As detailed in section 4, every palmprint image is described by 1×72 dimension feature vector. The identification of palmprint into one of the several known categories achieved by computing the similarity measure between the corresponding feature vectors.

2.1. Extraction of region of interest

The composite hand images are assumed to be acquired with the uniform background. These images are first binarized by subjecting the image to the discriminant analysis using image histogram [6]. Since the background and lighting conditions during the acquisition of images remain relatively constant, the thresholding limit is computed just for one image and used subsequently.

The binarized image is subjected to the morphological erosion to compute the region of interest. Let R be the set of non-zero pixels in a given binary image and SE be the set of non-zero pixels *i.e.* structuring element. The morphological erosion is defined as

$$R \Theta SE = \{g : SE_g \subseteq R\} \quad (1)$$

where SE_g denotes the structuring element with its reference point shifted by g pixels. A square structuring element (SE) is used to probe the composite binarized image. In our experiments 290×290 pixel palmprint images were used and therefore 145×145 pixels SE was found appropriate and used. The center of this residual image *i.e.* the center of rectangle that can enclose the residue is determined. These center coordinates are used to extract a circular palmprint region of fixed size from the composite hand image. The steps of this method can also be seen in the figure 2.

2.2. Normalization

The extracted palmprint images are normalized to have pre-specified mean and variance. The method of normalization used in this work is computationally simpler and is sufficient for the quality of acquired inkless images. The mean (ϕ) and the variance (ρ) of image $I(i,j)$ are used to compute the normalized image $I'(i,j)$:

$$I'(i,j) = \begin{cases} \phi_d + \lambda & \text{if } I(i,j) > \phi \\ \phi_d - \lambda & \text{otherwise} \end{cases} \quad (2)$$

$$\text{where } \lambda = \sqrt{\frac{\rho_d \{I(i,j) - \phi\}^2}{\rho}} \quad (3)$$

Proceedings of the Third International Conference on Image and Graphics (ICIG'04)
0-7695-2244-0/04 $20.00 © 2004 **IEEE**

where ϕ_d and ρ_d are the desired values for mean and variance. These values are pre-tuned according to the image characteristics *i.e.* $I(i,j)$. In all our experiments, the values of ϕ_d and ρ_d were fixed to 100. Figure 3 shows a typical palmprint image before and after the normalization.

3. Multichannel filtering

In spatial domain, the RGF filter is a Gaussian function modulated by an oriented cosine function. The impulse response RGF in 2D plane has following general form [5]

$$h(x', y') = \exp\left[-\frac{1}{2}\left(\frac{x^2}{\sigma_x^2} + \frac{y^2}{\sigma_y^2}\right)\right] \cos(2\pi u_0 x) \quad (4)$$

where $x' = x\sin\varphi + y\cos\varphi$, $y' = x\cos\varphi - y\sin\varphi$, and u_0 denotes the radial frequency of sinusoidal plane wave along direction φ from x axis. The space constants σ_x and σ_y define the Gaussian envelope along x- and y-axes respectively. In this work, the parameters of RGF were empirically determined using employed 100 dpi palmprint images. These were set as; $u_0 = 1/10$, and $\sigma_x = \sigma_y = 4$. The RGF filters were implemented as 13×13 spatial masks with six different values of $\varphi(0^0, 30^0, 60^0, 90^0, 120^0, 150^0)$. Thus every palmprint image is filtered with a bank of six RGF filters to generate six filtered images. Each of the filtered images (figure 4) accentuates the prominent palmprint lines and creases in corresponding direction (φ) while attenuating background noise and structures in other directions.

4. Extraction of features

The local gray level variations in the filtered images form the unique palmprint features. Despite our efforts to acquire the palmprint images in a preferred direction, some misalignment was inherently noticed and this can be attributed to the stretching, rotation, or shifting of palm by user on the sensor. Therefore local gray level variations in filtered images were sampled from concentric and overlapping bands. The usage of circular concentric bands was motivated by ring projection algorithm [8] which can be useful to achieve rotational invariance. The overlapping of concentric circular bands helps to reduce the effects of palm stretching. In this work, we used the variance and mean of gray levels in the concentric circular bands to capture the significant features. The mean value of ring projection vectors for every filtered image $I'_\varphi(i, j)$ in the circular band between radius r_1 and r_2 is obtained as follows;

$$\mu_\varphi^p = \frac{1}{N_r}\sum_r\sum_q I'_\varphi(r\cos\theta_q, r\sin\theta_q), \; p = 1,2,\ldots Z \quad (5)$$

where Z is the total number of circular bands and N_r is the total number of pixels falling between the circle of radius r_1 and r_2. The variance of local gray level pixels is also determined.

$$\sigma_\varphi^p = \sqrt{\frac{1}{N_r^2}\sum_r\sum_q \left(I'_\varphi(r\cos\theta_q, r\sin\theta_q) - \mu_\psi^p\right)^2} \quad (6)$$

The ordered set of these features, *i.e.* (5) and (6), from each of the six filtered images, is used to obtain a unique feature vector as follows:

$$\Omega_k = \left\{\mu_\varphi^p, \sigma_\varphi^p\right\}, \quad \forall\, p = 1,2,..,Z, \; \varphi = 0^0, 30^0, \ldots 150^0. \quad (7)$$

This composite feature vector carries the discriminatory information from each of the palmprints and is here referred to as *PalmCode,* which is similar to *FingerCode* or *IrisCode* used in the literature [7].

5. Identification

The *PalmCodes* for every possible user, from their palmprint training images, is used to build a training database or matrix $\mathbf{\Omega}$, *i.e.*,

$$\mathbf{\Omega} = [\Omega_1, \Omega_2, \ldots, \Omega_N] \quad (8)$$

where N is the total number of valid users. Each of these feature vector is unique and posses the discriminatory information. During recognition, the characteristic feature vector, say Λ, of an unknown user is obtained by using (7). This vector is compared with each of the feature vector of k^{th} user *i.e.* Ω_k. The class label with best possible match is assigned to unknown user. The maximum similarity between the feature vectors in matrix $\mathbf{\Omega}$ and query vector Λ is determined as follows:

$$\beta_{\max} = \max_k \left\{ \frac{\sum_l \Lambda\Omega_k}{\sqrt{\sum_l \Lambda \sum_l \Omega_k}} \right\}, \; l = 1,2,\ldots,6Z, \; k = 1,2,\ldots,N \quad (9)$$

The class label corresponding to the vector Ω_k that generates highest score, *i.e.* $\beta_{\max}$, is assigned to the *PalmCode* Λ of unknown user.

6. Experiments and Results

The experimental results reported in this paper were performed on a set of 800 images acquired from the 40 subjects, 10 each from the right- and left-palm, using HP-ScanJet ADF scanner. The users were requested to align their palm in a preferred direction, *i.e.*, the outward boundary of palm below the smallest finger is parallel to the alignment mark on the scanner. These two alignment marks on the scanner were provided at the left and right scanner boundaries. The different palmprint images varied mainly due to the stretching of palms, pressure on the scanner, and slight misalignment (rotation) of the palm. Only one palmprint image from each of the users was used for training and remaining for the testing. The recognition performance was evaluated on (*a*) left-

palmprint images, (*b*) right-palmprint images, and (*c*) when the right- and left-palmprint images from a user are assumed to be belonging to the two different users. Every filtered image was divided into six (Z=7) concentric circular bands. Each of these circular bands was 20 pixels wide and overlapped by 25%. The first circular band around the center was ignored.

The experimental results for recognition using palmprint images were encouraging. The visual representation of a typical *PalmCode* obtained from a palmprint image is shown in figure 5. The *PalmCode* is shown as 12 gray level images. Each pair of these discs corresponds to one filtered image. The gray level in each circular band of the disc represents the feature value for that band in the corresponding filtered image. Table 1 show the maximum recognition rate obtained from test dataset. It can be observed that the proposed scheme can recognize palmprints quite accurately as the maximum recognition rate of 97.50% has been obtained from the 40 class experiments. Table 1 also shows the results when the minimum Euclidean distance, instead of the maximum similarity, was used to recognize *PalmCodes*. The results show that the performance of similarity measure is superior to that based on Euclidean distance and was therefore used in all other experimental results reported in this paper. The false accept rate (FAR) and false reject rate (FRR) curves for three cases are shown in figure 6. The crossover error rate for 80 class experiment (case *c*) is 3.03 and is achieved at a specific threshold of 0.992. Figure 6 also shows the receiver operating characteristics (ROC) for the verification experiments. It can be noticed from this figure that the performance for 80 class experiments is better than those from 40 classes (*a* or *b*).

7. Discussion and Conclusions

This paper has investigated a new method of palmprint-based personal identification using RGF filters. The computational complexity of the proposed method is about half that of method in [4] mainly due to the usage of RGF mask of size 13×13 instead of complex Gabor filter masks of 31×31 sizes used in [4]. The reliability on the performance of a personal recognition system largely depends on its degree of tolerance due to rotation, translation, and scaling. The *PalmCode* representation used in this work is not rotation invariant. However, the rotation can be well handled by the rotation of *PalmCode* during the verification/recognition stages. This can be achieved by only using the best similarity measure (9) computed from the cyclic rotation of the *PalmCode* to be verified or recognized. The extent of translation (mainly due to palm stretching) invariance is accomplished by overlapping the concentric circular bands.

The experimental results show that the performance for the combination of two palmprints (case *c*) is better than the case when two palmprints are separately utilized. This is intuitively expected as the discrimination offered for case (*c*) is much higher as the orientation of all palm lines and creases in two palms are different/opposite. Thus the combination of two palmprints of same subject cannot be used to estimate the equivalent performance for two subjects. Therefore the experimental results obtained in [4], concurrently with this study, were biased and does not represent the actual performance. In our experiments, the rotation and translation of palmprints was restricted during the image acquisition as the alignment marks were provided on the sensor used for acquiring the images. The problem of scale invariance is automatically fixed once a particular image sensor, at a fixed resolution, is employed during user registration and identification. However a periodic update of training database is required to tackle the scale change due to physiological growth. One possible solution is to update the training database from the users, every time a user is positively verified by the system. The accuracy of experimental results shown in this paper may be limited due to small size of available database and therefore our future work will focus on the performance evaluation using large size database.

8. References

[1] N. G. Altman, "Palm print identification system," *U. S. Patent No*. 3,581,282, 1971.

[2] Nassimbene, "Palm print identification," *U. S. Patent No*. 4,032,889, 1977.

[3] S. Wei, *Research on Automatic Palmprint Recognition*, Ph.D. Thesis, Tsinghua University, 1999.

[4] D. Zhang, W.K. Kong, J. You, and M. Wong, "On-line palmprint identification" *IEEE Trans. Patt. Anal. Machine Intell*., vol. 25, pp. 1041-1050, Sep. 2003.

[5] A. Kumar and G. Pang, "Fabric defect segmentation using multi-channel blob detectors," *Optical Engineering*, vol. 39, pp. 3176-3190, Dec. 2000

[6] N. Otsu, "A threshold selection method from gray-scale histogram," *IEEE Trans*. *Syst*., *Man*, *Cybern*., vol. 8, pp. 62-66, 1978

[7] J. G. Daugman, "High confidence recognition of persons by a test of statistical independence," *IEEE Trans. Patt. Anal. Machine Intell.*, vol. 15, pp. 1148-1161, Nov. 1993.

[8] D.-M Tsai and C.-H. Chiang, "Rotation-invariant pattern matching using wavelet decomposition," *Pattern Recognit. Lett*., vol. 23, pp. 191-201, Jan. 2002.

Table 1: Maximum recognition rate from the experiments.

Recognition Rate (%)	Using Similarity measure	Using Euclidean distance
Both palm (80 class)	98.00	91.50
Right palm (40 class)	96.75	90.50
Left palm (40 class)	97.50	91.00

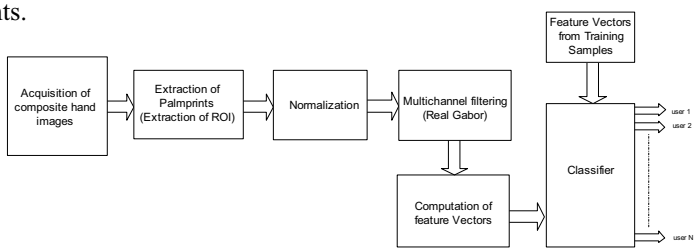

Figure 1: Block diagram of experimental setup.

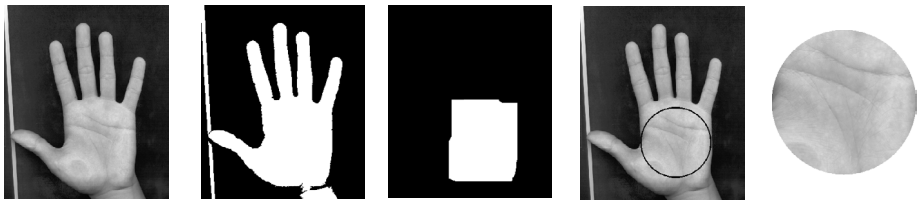

Figure 2: (a) Acquired image from the image sensor, (b) image after thresholding, (c) image residue after morphological erosion, (d) circular region of interest generated from the limits of image (c), (e) segmented palmprint image.

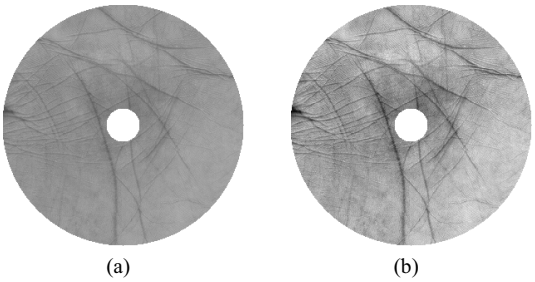

Figure 3: Palmprint image before (a) and after (b) normalization.

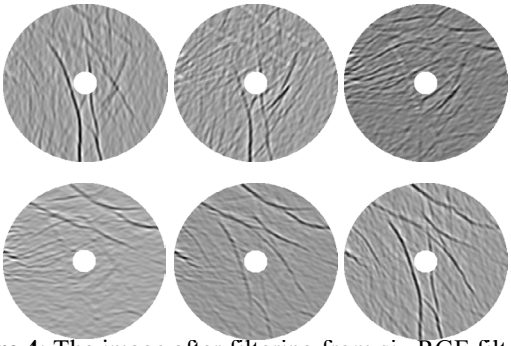

Figure 4: The image after filtering from six RGF filters.

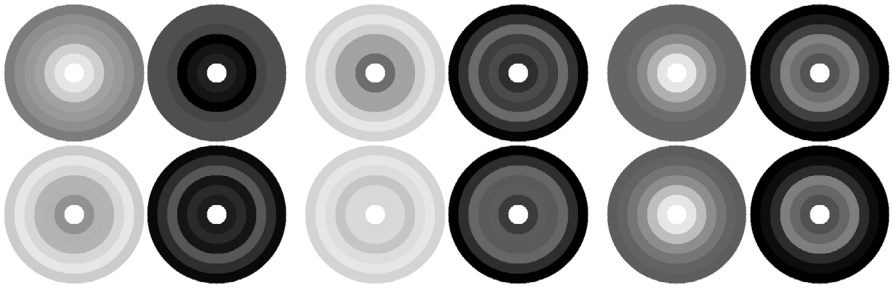

Figure 5: *PalmCode* for a typical palmprint used in the experiments.

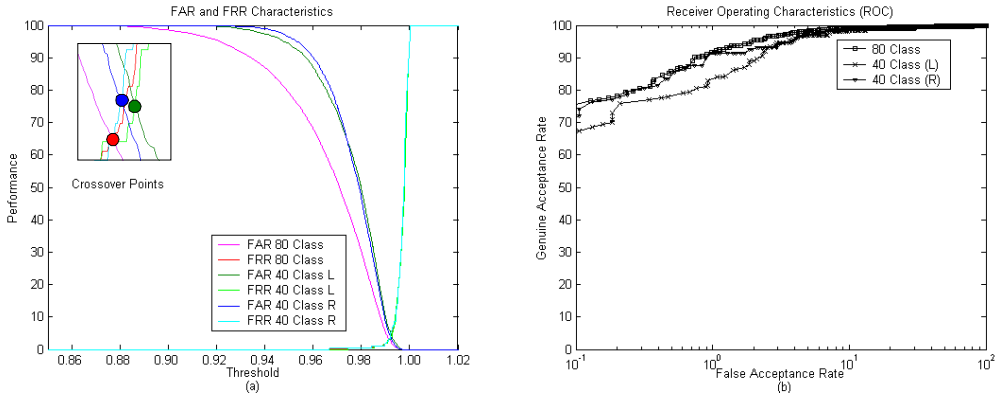

Figure 6: (a) The FAR and FRR characteristics; (b) The ROC from the verification experiments.